PHYSICAL REVIEW B VOLUME 60, NUMBER 4 15 JULY 1999-II

Nanometer ripple formation and self-affine roughening of ion-beam-eroded graphite surfaces

S. Habenicht, W. Bolse,* and K. P. Lieb
II. Physikalisches Institut and Sonderforschungsbereich 345, Georg-August-Universität Göttingen, Bunsenstrasse 7-9, D-37073 Göttingen, Germany

K. Reimann and U. Geyer
I. Physikalisches Institut and Sonderforschungsbereich 345, Georg-August-Universität Göttingen, D-37073 Göttingen, Germany

(Received 20 April 1999)

The topography of (0001)-graphite (highly oriented pyrolytic graphite) surfaces eroded by a 5 keV Xe^+ ion beam has been investigated using scanning tunneling microscopy. For tilted incidence of the ion beam and ion fluences of about 10^{17} cm^{-2}, a quasiperiodic ripple topography with characteristic wavelengths between 40 and 70 nm has been found. As predicted by continuum theory and Monte Carlo simulations, below a critical angle θ_C the ripples are oriented perpendicular to the ion beam projection onto the surface, while for angles above θ_C the ripple orientation is parallel to the ion beam projection. The critical angle θ_C lies between 60° and 70°, in agreement with the predictions of the continuum theory. For rising ion fluences, large scale perturbations of the surface topography occur indicating a nonlinear behavior governed by the Kardar-Parisi-Zhang universality class. [S0163-1829(99)50628-0]

The evolution of solid surface topography during ion-beam sputtering is governed by the interplay and competition between the dynamics of surface roughening on the one hand and material transport during surface diffusion on the other. It is, therefore, seen in analogy to surface evolution processes during film growth.[1,2] Surface diffusion is driven by the minimization of the surface energy and acts like a ''positive surface tension.'' In contrast, the removal of atoms during ion-beam treatment roughens the surface because of the curvature dependence of the sputter yield, which is described as a so-called ''negative surface tension.'' These processes compete during ion beam erosion and are responsible for the creation of characteristic surface patterns like self-affine topographies[3,4] and quasiperiodic ripples,[5–10] when the ion-beam is tilted to the surface normal.

Theoretically the evolution of the morphology has been investigated by Bradley and Harper[11] and more generally by Cuerno and Barabasi[2,12] and Rost and Krug.[13] According to the continuum theory of ion-beam sputtering by Sigmund,[14,15] the authors developed a model of surface erosion in terms of a generalized anisotropic Kuramoto-Sivashinsky equation. This theory predicts the evolution of quasiperiodic surface ripples at intermediate ion fluences when local slopes of the surface are moderate (described as the linear regime). The ripple orientation should be perpendicular to the beam direction (which is defined as the y direction of the surface) for incidence angles less than a critical angle θ_c, and parallel (defined as the x direction of the surface) to the beam direction for incidence angles close to grazing. Recent Monte Carlo simulations on ion-beam-eroded carbon surfaces by Koponen *et al.*[16,17] indeed predict surface ripple morphologies with nanometer scales ($\lambda = 15-40$ nm) and the switching of the ripple orientation when tilting the incidence angle θ. Apart from that, for large ion fluences the increase of the local slopes of the surface topography should lead to a nonlinear behavior of the evolution of the surface morphology with self-affine scaling. This transition has been modeled in simulations in the case of $1+1$ dimensions by Cuerno *et al.*,[18] who argued that the pattern is characterized by a crossover to a rough surface in the universality class of the Kardar-Parisi-Zhang (KPZ) equation.[19].

Ripple morphology in different dimensions has been observed experimentally on various eroded surfaces[5,7–10] and self-affine scaling of surface morphologies has been investigated using scanning electron (SEM) and scanning probe microscopy (STM and AFM). However, a comparison with theoretical models has been aggravated by the fact that the ripple dimensions were difficult to compare to the predictions of the continuum model and especially that the critical angle θ_C of the ripple rotation was not observed clearly in the previous measurements. Recently, Rusponi *et al.* reported on the rotation of ripples on Cu(110) surfaces after ion bombardment.[20] In those measurements, the ripple orientation and the critical angle are perturbed by the effect of Ehrlich-Schwoebel barriers in different crystallographic directions. It is the aim of this paper to present results on ion-beam-eroded graphite surfaces with ripple morphologies which can be related, for the first time to the author's knowledge, to the results of Monte Carlo simulations, to prove changing of the ripple orientation with the incidence angle and to compare quantitatively the experimental results and the theoretical predictions of the ripple structures. Due to its low critical dose of amorphization,[21] the effects of anisotropy in surface diffusion and Ehrlich-Schwoebel barriers can be neglected on graphite surfaces and so the effects are comparable to the theory. Furthermore, experimental indications of the transition from the linear to the nonlinear regime with rising ion fluence will be presented, which has not been experimentally observed up to now.

The experiments were performed using freshly cleaved graphite [highly oriented pyrolytic graphite (HOPG)] surfaces with (0001)-orientation. The samples were irradiated at 300 K with Xe^+ ions by the Göttingen IOSCHKA

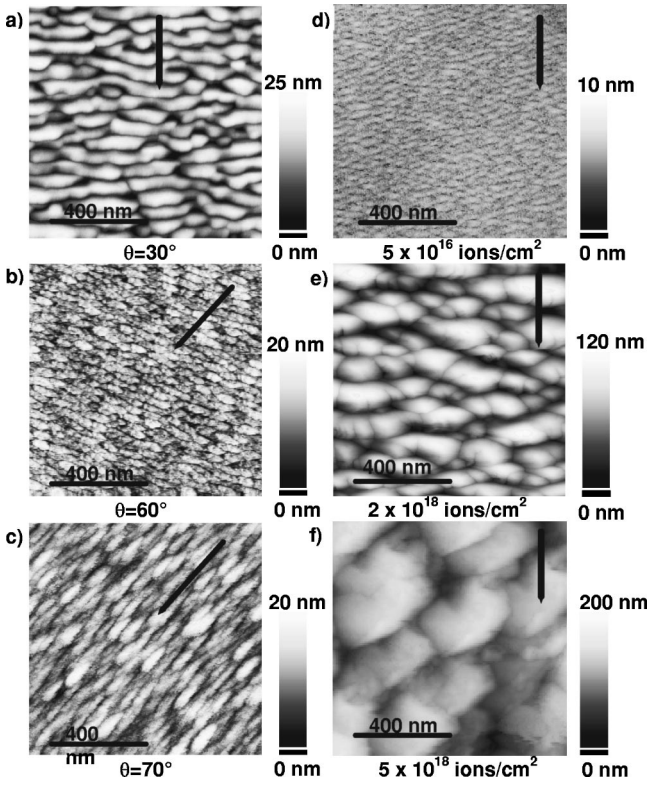

FIG. 1. STM micrographs (lateral size 1 μm) of 5 keV Xe^+ eroded HOPG surfaces. Left column (a)-(c): irradiation fluence $\Phi = 3\times10^{17}$ ions/cm^2; incident angle θ (a) 30°, (b) 60°, (c) 70°. Right column (d)–(f): incident angle $\theta = 60°$; irradiation fluence Φ (d) 5×10^{16} ions/cm^2, (e) 2×10^{18} ions/cm^2, (f) 5×10^{18} ions/cm^2. Arrows indicate the ion-beam orientation. Height scales are added for each picture.

implanter.[22] An ion energy of 5 keV and an implantation fluence between 5×10^{16} and 6×10^{18} cm^{-2} were chosen to realize the conditions of the simulations. The ion flux was kept constant at 15 μA/cm^2 for all implantations, the angle of incidence (relative to the surface normal) was varied between 0° and 80°. Homogeneous implantation was achieved via two-dimensional electrostatic sweeping. After irradiation, the samples were investigated under ambient conditions, using mechanically prepared $Pt_{80}Ir_{20}$ tips and a Nanoscope-STM (Digital Instruments) to observe the evolution of height profile.

Figure 1 shows STM micrographs of HOPG surfaces irradiated for different incident angles at an Xe^+-ion fluence of 3×10^{17} cm^{-2} [(a)–(c): left column] and for different ion fluences at an incident angle of $\theta = 60°$ [(d)–(f): right column]. As clearly visible in the left column, a periodic ripple morphology evolves when the ion beam is tilted to the surface normal. As the erosion depth of ca. 150 nm exceeds the typical implantation depth of 5 keV Xe^+ ions in graphite (ca. 7 nm) by more than an order of magnitude, bulk effects (spikes, dislocations, bubbles, etc.) as reported for Ge and other systems[23] can be excluded to be responsible for this rippling phenomenon, which therefore must be related to surface sputtering. For $\theta = 30°$ and 60°, the ripples are oriented perpendicular to the ion-beam surface projection, which means that the wave vector $\mathbf{k}$ is oriented parallel to the ion beam projection. For $\theta = 70°$ the ripple orientation has rotated by 90° and the ripples are now oriented parallel to the ion-beam projection. Therefore the critical angle θ_C for 5 keV Xe^+ ions on graphite (HOPG) is determined to be between $\theta = 60°$ and $\theta = 70°$. For detailed analyses of the STM pictures (wavelengths, local slopes, etc.) the structure factor $S(\mathbf{k})$ of the height topography $h(\mathbf{r},t)$ was computed:

$$S(\mathbf{k}) = |\hat{h}(\mathbf{k})|^2 \tag{1}$$

and

$$\hat{h}(\mathbf{k}) \propto \int_{\mathbf{r}} \exp[i\mathbf{kr}][h(\mathbf{r}) - \overline{h}]d\mathbf{r}.$$

For $\theta < \theta_C$, $S(\mathbf{k})$ was calculated for cuts through the STM pictures along the ion-beam direction, for $\theta > \theta_C | S(\mathbf{k})$ was calculated perpendicular to the ion-beam projection onto the surface. The maximum of the structure factor $S(\mathbf{k})$ corresponds to the observed wavelength. For $\theta \leqslant 60°$, wavelengths of $\lambda_x(30°) = 67(9)$ nm, $\lambda_x(45°) = 50(9)$ nm, and $\lambda_x(60°) = 45(8)$ nm were found, while for $\theta = 70°$ a wavelength of $\lambda_y(70°) = 60(9)$ nm was determined. These ripple dimensions agree, within a factor of 2, with the results of the Monte Carlo simulations.[16] However, as long as the surface mobility B is merely known to within an order of magnitude, the wavelength cannot exactly be determined theoretically. Nevertheless the experimental ratios of wavelengths at different incident angles, $\lambda(\theta_1)/\lambda(\theta_2)$, and the experimentally found critical angle θ_C has to be reproduced by the linear continuum theory. For this purpose the distribution of the deposited energy (according to Bolse[24]) of 5 keV Xe^+ in carbon was calculated by simulating the atomic displacement cacade using the TRIM95 (transport of ions in matter) code.[25] The energy distribution can be characterized by the mean depth a and the longitudinal and a lateral straggling α and β. In this case the three parameters were determined to be $a = 3.2$ nm, $\alpha = 2.0$ nm, and $\beta = 1.0$ nm. These values enter the coefficients of curvature dependent sputtering $\Gamma_{x,y} = \Gamma_{x,y}(a,\alpha,\beta)$ in the description by Bradley and Harper,[11] where $\lambda \propto \sqrt{B/|\Gamma_{x,y}|}$. The wavelengths λ_x and λ_y perpendicular and parallel to the ion-beam projection as calculated by

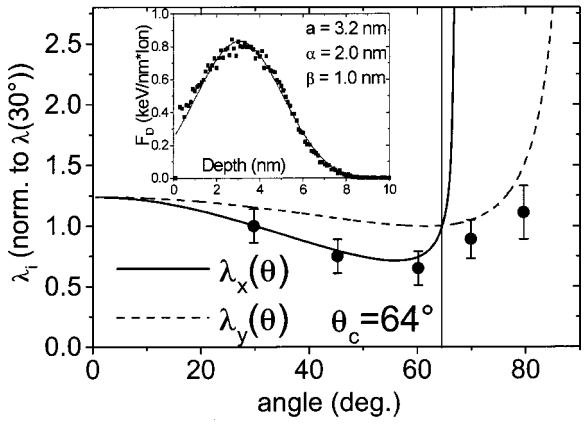

FIG. 2. Angular dependence of the wavelengths $\lambda_{x,y}$ as calculated from the linear continuum theory. The functions are normalized to $\lambda(30°)$. Experimental values are added for comparison. The distribution values of deposited energy were taken from TRIM calculations (shown in the inset).

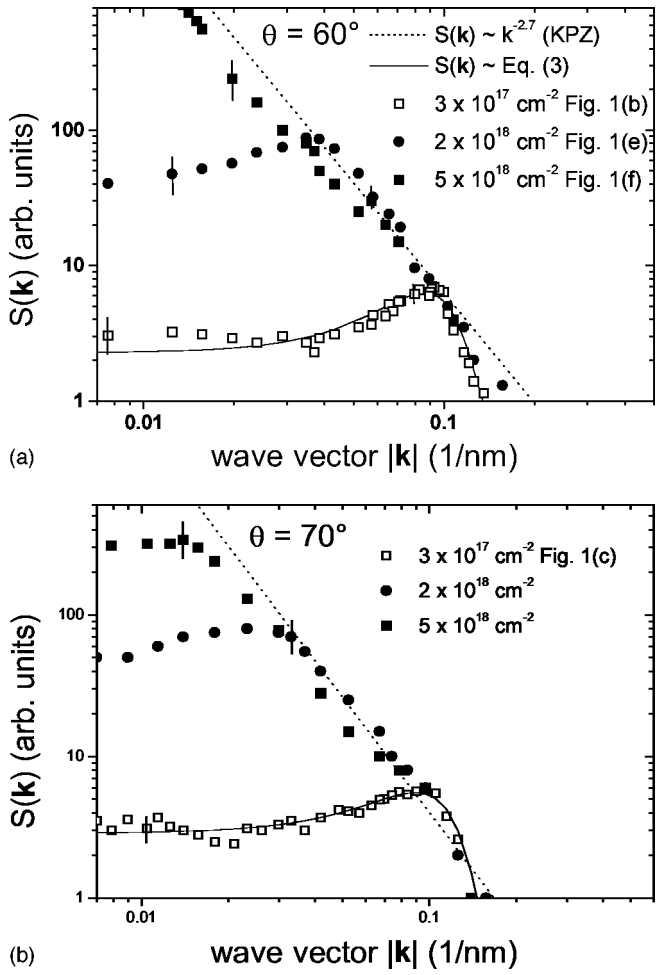

FIG. 3. Structure factor $S(\mathbf{k})$ calculated from STM pictures with rising ion fluence at 60° (left) and 70° (right) incidence angle. The solid line represents a fit to the data according to Eq. (3). The dashed line shows the power dependence of $S(\mathbf{k})$ according to KPZ-universality class.

the continuum theory are presented in Fig. 2. The experimental ratios $\lambda_x(60°)/\lambda_x(30°)=0.65(14)$, $\lambda_x(45°)/\lambda_x(30°)=0.75(14)$, $\lambda_y(70°)/\lambda_x(30°)=0.89(15)$ are in good agreement with the values obtained by the linear continuum theory $\lambda_x(60°)/\lambda_x(30°)=0.73$, $\lambda_x(45°)/\lambda_x(30°)=0.82$ and $\lambda_y(70°)/\lambda_x(30°)=1.05$. The theoretically expected critical angle $\theta_C=64°$ reproduces the experimentally found change in the ripple orientation between 60° and 70°. In this fluence regime the surface height evolution $h(\mathbf{r},t)$ follows the differential equation

$$\frac{\partial h}{\partial t}=-F_0+C\frac{\partial h}{\partial x}+\Gamma_x\frac{\partial^2 h}{\partial x^2}+\Gamma_y\frac{\partial^2 h}{\partial y^2}-B\nabla^4 h+\eta. \quad (2)$$

F_0 defines the surface erosion rate at normal incidence, $C\partial h/\partial x$ is a term related to the derivative of the sputtering yield with respect to the angle of incidence, $\Gamma_{x,y}\partial^2 h/\partial x,y^2$ describes the curvature dependence of the surface erosion, $B\nabla^4 h$ the surface diffusion according to Wolf-Villain, and η denotes the noise terms.[12] The structure factor $S(\mathbf{k})$ can then be analytically expressed by a superposition of the linear evolution described by Bradley and Harper and stochastic roughening ω,[5,7,10]

$$\frac{d|\hat{h}(\mathbf{k})|^2}{dt}=R_k|\hat{h}(\mathbf{k})|^2+\omega,$$

$$S(\mathbf{k})=|\hat{h}_0(\mathbf{k})|^2\exp(R_k t)+\frac{\omega}{R_k}[\exp(R_k t)-1]$$

$$\text{with}\quad R_k=-C|\mathbf{k}|-\Gamma|\mathbf{k}|^2-B|\mathbf{k}|^4. \quad (3)$$

For all angles, the structure factor calculated in this fluence regime according to Eq. (3) is in good agreement with the experimental curves as indicated in Fig. 3. When comparing the maximum slopes at the ripple flanks of both the STM pictures and the Monte Carlo simulations, the experimental values vary between 15° and 30°, about twice as high as the values found in the simulations (7°−14°). This deviation and also the differences in the wavelengths between experiments and Monte Carlo simulations may be explained by the surface diffusion underestimated by the model of Wolf-Villain, since it only includes diffusion-induced surface relaxation between nearest and next-nearest neighbors.[26]

The good agreement of the structure factors of the STM pictures and Eq. (3) at low fluences was used to test the continuum theory in the higher fluence. For increasing fluence Φ the periodic ripple morphology was found to dominate [see Fig. 1(d)] between $\Phi=5\times10^{16}$ cm^{-2}, where weak surface contours are visible, and $\Phi=5\times10^{17}$ cm^{-2}, where the ripple topography is fully developed. When the ion fluence is further increased, one observes a loss of the periodic structure and its orientation relative to the ion-beam direction [see Figs. 1(e) and 1(f)]. This development is caused by the growth of long-range surface instabilites as visible in the evolution of the structure factors $S(\mathbf{k})$ presented in Fig. 3 for incidence angles of $\theta=60°$ and $\theta=70°$. $S(\mathbf{k})$ was calculated in the same way as described in the linear regime. For increasing fluence, the long-range perturbations with wavelengths $\lambda>\lambda_C\propto\sqrt{B/|\Gamma_{x,y}|}$ grow faster than the short-wave perturbations and shift the maximum of $S(\mathbf{k})$ to smaller wave vectors. The approximation of the structure factor according to the linear theory [Eq. (3)] is no longer valid and the wave pattern vanishes finally. This behavior is typical for the nonlinear surface evolution described by the universality class of the KPZ equation.[19,27] According to renormalization theory one should observe an algebraic scaling behavior[12]

$$S(\mathbf{k})=|\hat{h}(\mathbf{k})|^2\propto|\mathbf{k}|^{-\nu}, \quad (4)$$

with the scaling exponent of $2<\nu<3$ depending on the coupling size, i.e. the influence of nonlinearity. At a fluence of 2×10^{18} cm^{-2} and 5×10^{18} cm^{-2} (see Fig. 3), one finds $\nu=2.7$ in agreement with the KPZ theory and with previous experiments.[3,4] This transition between the linear regime, with its competition of surface erosion and diffusion and the formation of ripple morphologies, and the nonlinear regime has been predicted by simulations to ''effectively take place in the time evolution of the *same* physical system.''[18] To confirm this picture, it would be of interest to see if this is a general phenomenon in the physics of surfaces eroded by ion beams.

We would like to thank I. Koponen and M. Rost for helpful discussions and suggestions. This work was funded by the Deutsche Forschungsgemeinschaft.

*Present adress: Insitut für Strahlenphysik, Universität Stuttgart, Allmandring 3, D-70569 Stuttgart, Germany.

[1] C.A. Lang, C.F. Quate, and J. Nogami, Appl. Phys. Lett. **59**, 1696 (1991).

[2] A.L. Barabasi and H.E. Stanley, *Fractal Concepts of Surface Growth* (Cambridge University Press, Cambridge, 1995).

[3] E.A. Eklund, R. Bruinsma, J. Rudnick, and R.S. Williams, Phys. Rev. Lett. **67**, 1759 (1991).

[4] J. Krim, I. Heyvart, D.V. Haesendonck, and Y. Bruynserade, Phys. Rev. Lett. **70**, 57 (1993).

[5] E. Chason, T.M. Mayer, B.K. Kellerman, D.T. McIlroy, and A.J. Howard, Phys. Rev. Lett. **72**, 3040 (1994).

[6] G. Carter, M.J. Nobes, F. Paton, J.S. Williams, and J.L. Whitton, Radiat. Eff. **33**, 65 (1977).

[7] T.S. Mayer, E. Chason, and A.J. Howard, J. Appl. Phys. **76**, 1633 (1994).

[8] G. Carter, V. Vishniyakov, and M.J. Nobes, Nucl. Instrum. Methods Phys. Res. B **115**, 440 (1996).

[9] G. Carter and V. Vishnyakov, Phys. Rev. B **54**, 17 647 (1996).

[10] R. Schlatmann, J.D. Shindler, and J. Verhoeven, Phys. Rev. B **54**, 10 880 (1996).

[11] R.M. Bradley and J.M.E. Harper, J. Vac. Sci. Technol. A **6**, 2390 (1988).

[12] R. Cuerno and A.L. Barabasi, Phys. Rev. Lett. **74**, 4746 (1995).

[13] M. Rost and J. Krug, Phys. Rev. Lett. **75**, 3894 (1995).

[14] P. Sigmund, J. Mater. Sci. **8**, 1545 (1973).

[15] P. Sigmund, in *Sputtering by Particle Bombardment*, edited by R. Behrisch (Springer-Verlag, Heidelberg, 1983).

[16] I. Koponen, M. Hautala, and O.P. Sievänen, Phys. Rev. Lett. **78**, 2612 (1997).

[17] I. Koponen, M. Hautala, and O.P. Sievänen, Nucl. Instrum. Methods Phys. Res. B **129**, 349 (1997).

[18] R. Cuerno, H.A. Makse, S. Tomassone, S.T. Harrington, and H.E. Stanley, Phys. Rev. Lett. **75**, 4464 (1995).

[19] M. Kardar, G. Parisi, and Y.C. Zhang, Phys. Rev. Lett. **56**, 889 (1986).

[20] S. Rusponi, G. Costantini, C. Boragno, and U. Valbusa, Phys. Rev. Lett. **81**, 2735 (1998).

[21] T. Venkatesan, B.S. Elman, G. Braunstein, M.S. Dresselhaus, and G. Dresselhaus, J. Appl. Phys. **56**, 3232 (1984).

[22] S. Habenicht, W. Bolse, and K.P. Lieb, Rev. Sci. Instrum. **69**, 2120 (1998).

[23] B.R. Appleton, O.W. Holland, D.B. Poker, J. Narayan, and D. Fathy, Nucl. Instrum. Methods Phys. Res. B **7/8**, 639 (1985); Appl. Phys. Lett. **41**, 711 (1982).

[24] W. Bolse, Mater. Sci. Eng., R. **12**, 53 (1994).The distribution of the deposited energy was estimated by calculating the distribution of displacements and replacements during the ion collision cascade.

[25] J.F. Ziegeler, J.P. Biersack, and K. Littmark, *The Stopping and Ranges of Ions in Solids* (Pergamon, New York, 1985).

[26] D.E. Wolf and J. Villain, Europhys. Lett. **13**, 389 (1990).

[27] J. Krug and H. Spohn, in *Solids Far from Equilibrium*, edited by C. Godreche (Cambridge University Press, Cambridge, 1991).